Dependence of AGN Activity on Halo Mass and Redshift in the SPT Cluster Surveys

Benjamin Floyd[1] Mark Brodwin[1] Rebecca E. A. Canning[2,3] The SPT Collaboration

[1]University of Missouri–Kansas City [2]Kavli Institute for Particle Astrophysics and Cosmology [3]Stanford University

Motivation

We know that environment plays a role in galaxy evolution (e.g., Dressler, 1980, 1984) but how exactly? What are the predominant environmental-dependent mechanisms that are behind the rapid mass assembly (Mancone et al., 2010), enhanced star formation (Brodwin et al., 2013) and increased AGN activity (Martini et al., 2013) that has been observed in galaxy clusters at high-redshift ($z \gtrsim 1.4$). Independently both Brodwin et al. (2013) and Ehlert et al. (2015) arrived at similar conclusions that galaxy-galaxy merging within the clusters may be the mechanisms driving galaxy evolution in galaxy clusters early in their history.

Similar to Ehlert et al. (2015), we aim to model the AGN incidence in galaxy clusters as tracers of galaxy evolution of the cluster members.

SPT Cluster Sample

Figure 1. SPT-CLJ2344-4243, the Phoenix Cluster, the most X-ray luminous cluster.

Our cluster sample derives from two galaxy cluster surveys carried out by the 10-meter South Pole Telescope (SPT; Carlstrom et al., 2011) the 2500 deg^2 SPT-SZ survey (Bleem et al., 2015) and the deep, 100 deg^2 SPTpol 100d survey (Huang et al., 2020). Combined we have a cluster sample of over 300 clusters with a median redshift of $z \sim 0.69$ and median cluster mass of $M_{500} \sim 3.73 \times 10^{14} M_{\odot}$.

By using the SPT cluster surveys we are able to span a wide range of redshifts (see Fig 2.) and as the SPT detects clusters using the Sunyaev–Zel'dovich Effect (SZE) we have an effectively uniform-selected mass sample.

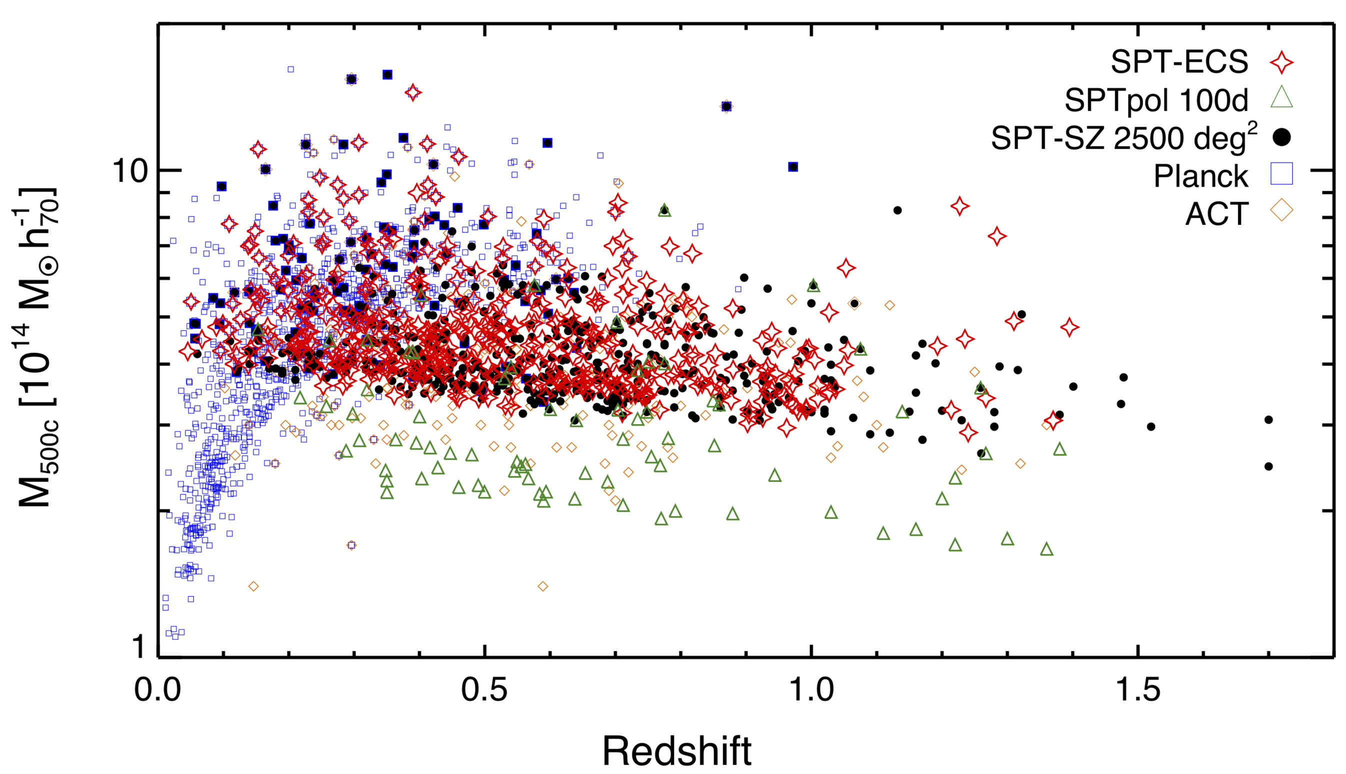

Figure 2. Mass and redshift distribution of the SPT cluster surveys.

Summary and Future Work

Using our model we are able to generate mock catalogs of IR-bright AGN along the line of sight of galaxy clusters with a wide range of physically motivated parameter values and for the number of galaxy clusters and AGN in our data sample we are able to constrain our input parameters with acceptable variances.

We have begun analysis of our data sample and preliminary results show indications of an inverse trend of AGN incidence with cluster mass but more work is to still to be done to confirm this trend.

IR-Bright AGN Selection

Our AGN are selected using *Spitzer*/IRAC imaging in $3.6\ \mu$m and $4.5\ \mu$m wavelengths. We find a color selection of $[3.6\ \mu\mathrm{m}] - [4.5\ \mu\mathrm{m}] \geq 0.7$ to be optimal in selecting AGN that would have been otherwise selected by a IRAC color-color selection (e.g., Stern et al., 2005) as shown in Figure 3.

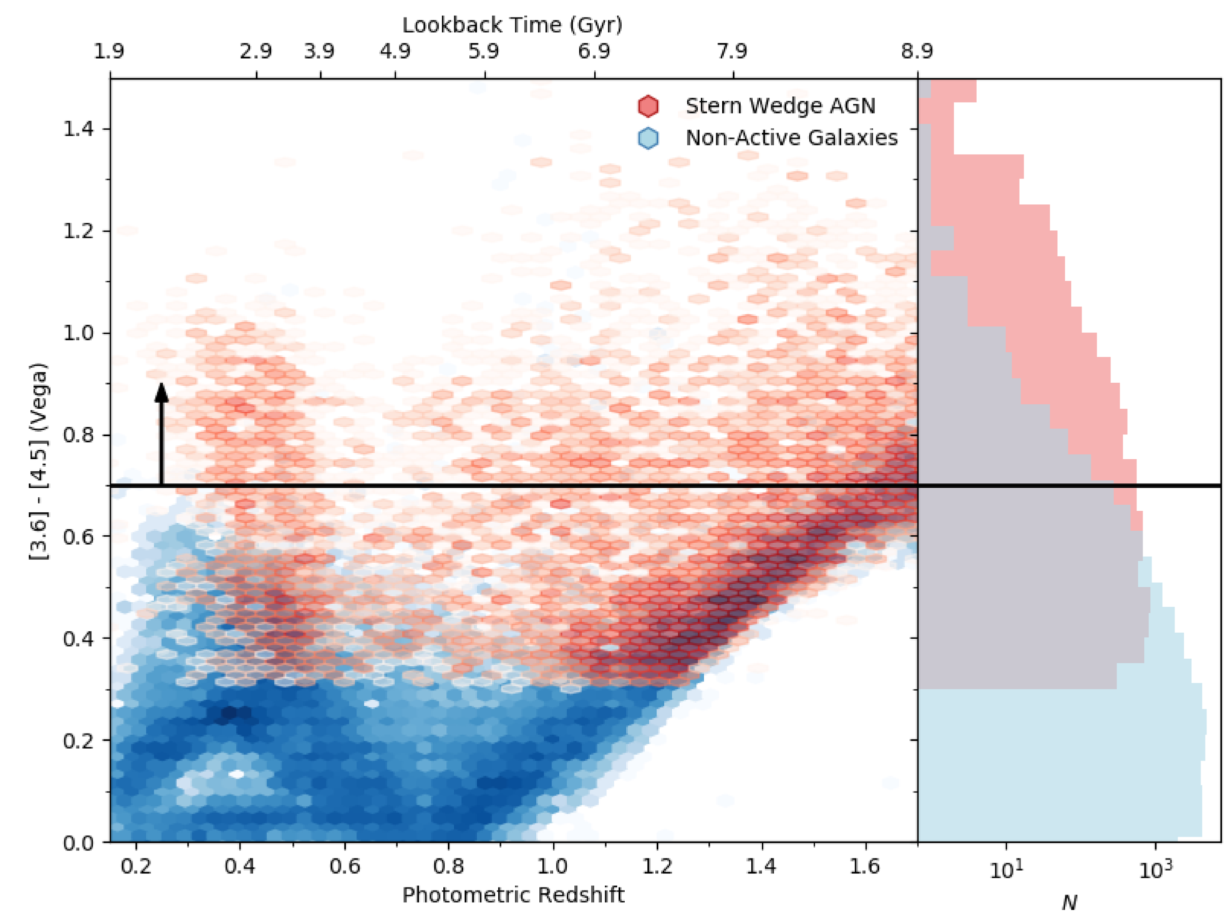

Figure 3. IRAC colors of all objects in the Spitzer Deep Wide-Field Survey (SDWFS; Ashby, Stern, et al., 2009) detected in $4.5\ \mu$m with SNR ≥ 5. Red points are objects that satisfy the AGN selection criterion as described in Stern et al. (2005). Blue hexbins are SDWFS objects that do not fall within the Stern wedge criterion. Our IRAC color selection is shown as the solid black line.

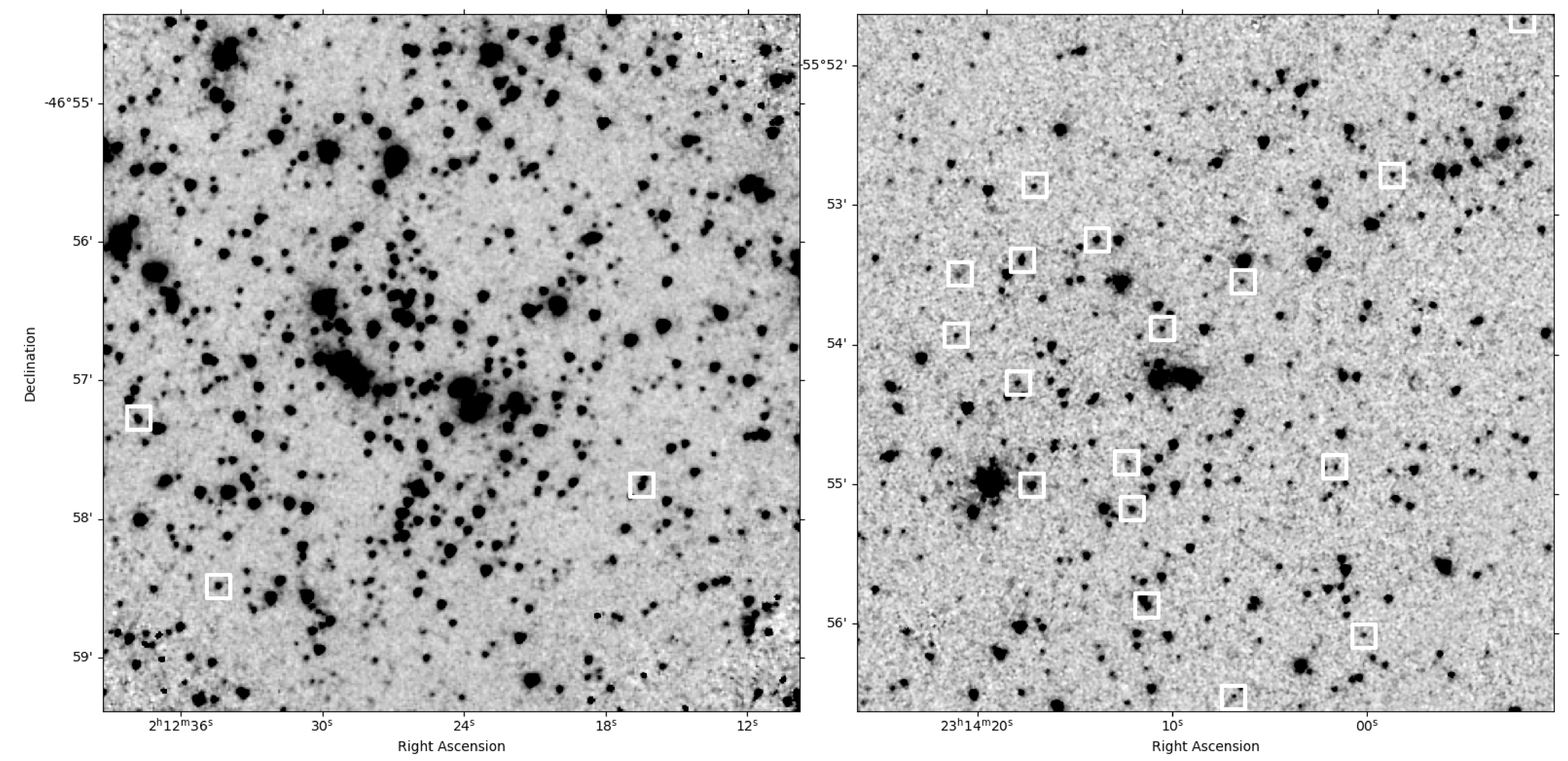

Figure 4. IRAC $3.6\ \mu$m images of SPT cluster around the median redshift of our sample. IR-bright AGN are marked by white boxes. (left) SPT-CL J0212-4657 $M_{500} = 6.06 \times 10^{14} M_{\odot}$, $z = 0.65$; (right) SPT-CL J2314-5554 $M_{500} = 2.18 \times 10^{14} M_{\odot}$, $z = 0.71$.

Bayesian Modeling

We model AGN incidence along the line-of-sight to a cluster as power laws in redshift and cluster mass and use a beta model to describe the projected cluster-centric radial distribution. The background contamination is modeled as a constant additive quantity.

Model

$$N(z, M_{500}, r) = \theta (1+z)^{\eta} \left(\frac{M_{500}}{10^{15} M_{\odot}}\right)^{\zeta} \left[1 + \left(\frac{r}{r_c}\right)^2\right]^{-1.5\beta+0.5} + C$$

Likelihood

$$\ln \mathcal{L}(\theta, \eta, \zeta, \beta, r_c, C) \propto \sum_j^{N_{\mathrm{cl}}} \left[\sum_i^{N_{\mathrm{AGN}}} \ln(N_{ji} r_i) - w_{\mathrm{comp}} \int_0^R N_j 2\pi r \, \mathrm{d}r\right]$$

To validate our probabilistic model and establish expected variances on model parameters we have created mock data sets that mimic our real data using model parameter sets chosen to test the expected parameter ranges.

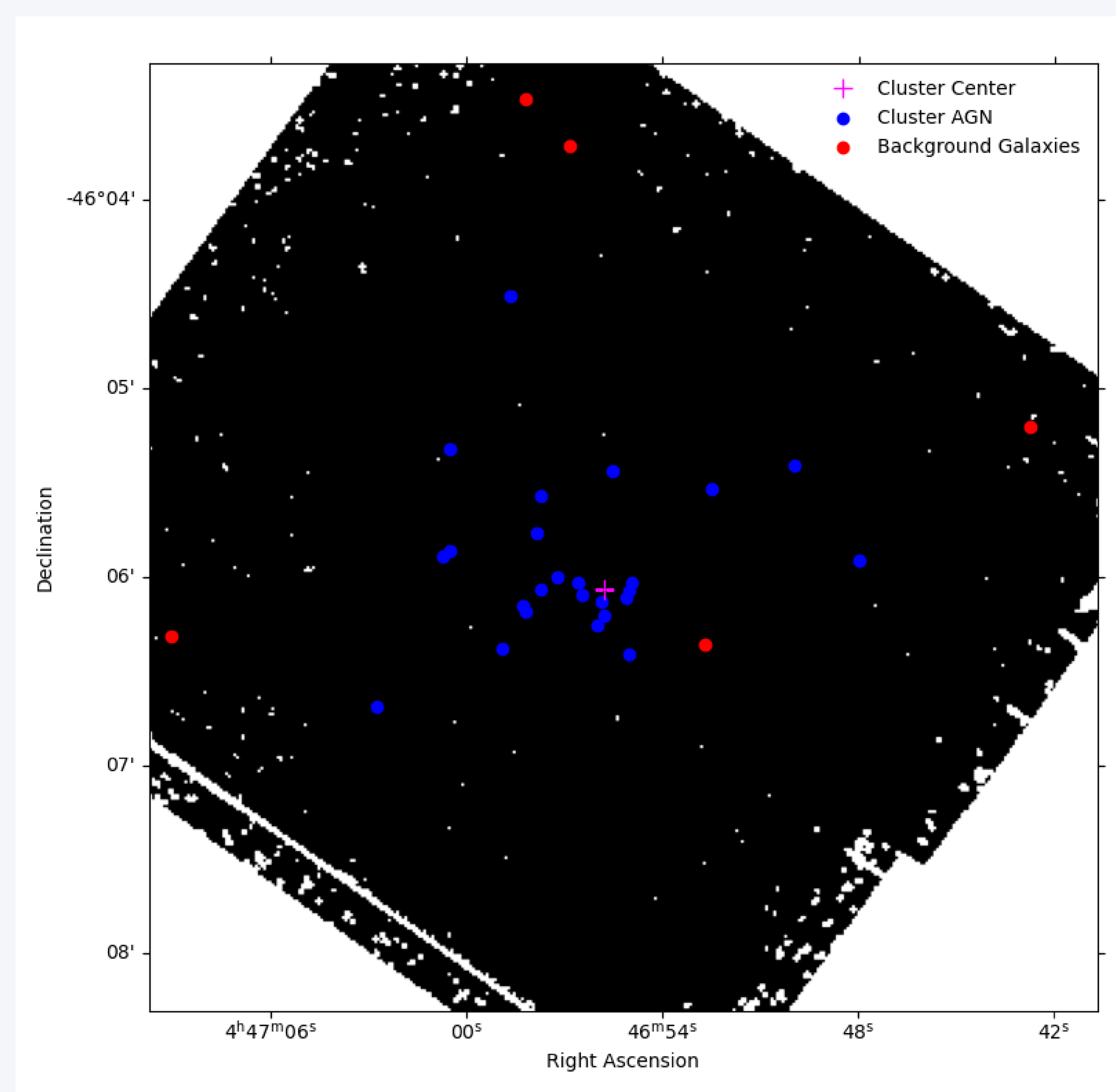

Figure 5. Example of a mock cluster with a background mask showing the area of the simulated image above our coverage threshold.

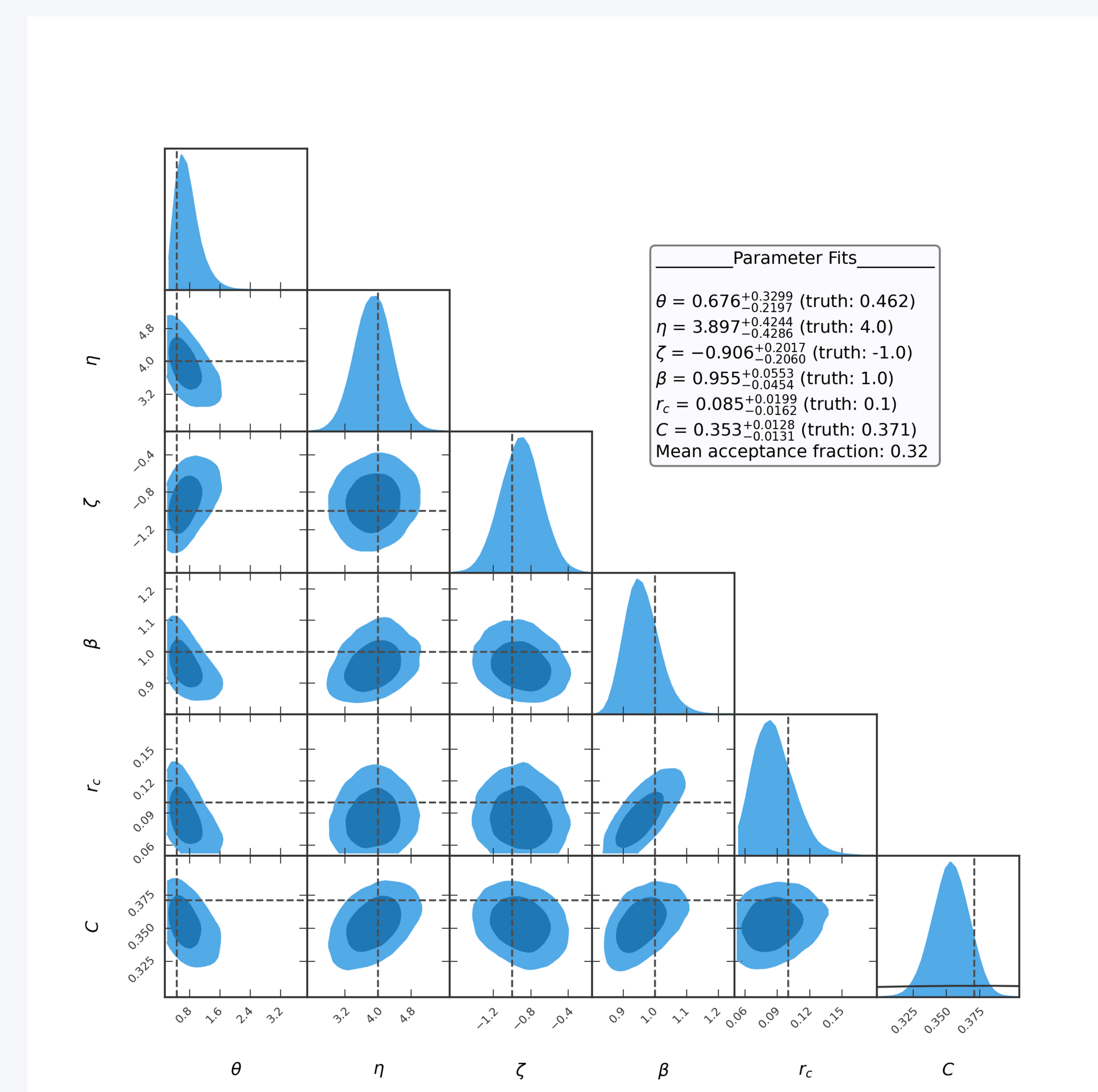

Figure 6. Model parameter fits from realistic mock catalog with input parameters indicated by dashed lines.

References

M. L. N. Ashby, S. A. Stanford, et al., ApJS **209**, 22, 22 (2013). M. L. N. Ashby, D. Stern, et al., ApJ **701**, 428 (2009). L. E. Bleem et al., ApJS **216**, 27, 27 (2015). M. Brodwin et al., ApJ **779**, 138, 138 (2013). J. E. Carlstrom et al., PASP **123**, 568 (2011). A. Dressler, ApJ **236**, 351 (1980). A. Dressler, ARA&A **22**, 185 (1984). S. Ehlert et al., MNRAS **446**, 2709 (2015). N. Huang et al., AJ **159**, 110, 110 (2020). C. L. Mancone et al., ApJ **720**, 284 (2010). P. Martini et al., ApJ **768**, 1, 1 (2013). D. Stern et al., ApJ **631**, 163 (2005).

btfkwd@umkc.edu